

An Embedded Boundary Method for Two Phase Incompressible Flow

S. Wang, J. Glimm, R. Samulyak, X. Jiao, and C. Diao

November 1, 2018

Department of Applied Mathematics and Statistics, Stony Brook University,
Stony Brook, NY 11794 USA

Contents

1	Introduction	2
2	The Projection Method	4
2.1	Projection Methods	4
2.1.1	Projection Method PM1	4
2.1.2	Projection Method PM2	5
2.1.3	Projection Method PM3	5
2.2	Time Discretization for the Calculation of the Intermediate Velocity	5
2.2.1	Crank-Nicolson Method	5
2.2.2	Additive Runge-Kutta Method	6
2.3	Calculation of the New Velocity	7
3	The EBM for Two-Phase Incompressible Flow	7
3.1	The Jump Conditions across an Internal Interface	7
3.2	The Embedded Boundary Method for the Elliptic Interface Problem	8
3.2.1	Discretization of the Jump Conditions	10
3.2.2	Equations for the Cell Center Unknowns	13
3.2.3	Geometric Property Calculation	13
3.3	The Embedded Boundary Method in Cylindrical Coordinates . .	14
3.3.1	Finite Difference Scheme for the Flux Calculation	15
3.3.2	Geometric Property Calculation	15
3.4	Calculation of the Pressure Gradient	16
3.5	The EBM for the Projection Step	16

4	Examples	17
4.1	Bubble Oscillation in Two and Three Dimension	17
4.1.1	Bubble Oscillation in Two Dimension	17
4.1.2	Bubble Oscillation in Three Dimension	18
4.2	EBM for the Elliptic Interface Problem in Cylindrical Coordinates	20
4.3	High Speed Two Phase Couette Flow	21
5	Conclusions	21
6	Acknowledgment	22
A	Approximate Jump Conditions for Decoupling Velocity	25
B	Code Structure and Parallelization	26

Abstract

We develop an embedded boundary method (EBM) to solve the two-phase incompressible flow with piecewise constant density. The front tracking method is used to track the interface. The fractional step methods are used to solve the incompressible Navier-Stokes equations while the EBM is used in the projection step to solve an elliptic interface problem for the pressure with a jump equal to the surface tension force across the interface. Several examples are used to verify the accuracy of the method.

1 Introduction

We consider here the two-phase incompressible Navier-Stokes equations (Zhijun Tan et al. [34])

$$\begin{aligned} \rho(u_t + (u \cdot \nabla)u) &= -\nabla p + \nabla \cdot \mu(\nabla u + (\nabla u)^T) + F(x, t) + g(x, t), \\ \nabla \cdot u &= 0, \end{aligned} \quad (1)$$

where ρ is the density (constant in each phase), u is the velocity field, p is the pressure, μ is the viscosity, $g(x, t)$ is the external body force and

$$F(x, t) = \int_{\Gamma} f(s, t)\delta(x - X(s, t))ds$$

is the singular interface force, concentrated on the interface with parametrization $X(s, t)$.

There are many different methods for solving the two-phase incompressible flow that also track the phase interface. Some of the most popular methods are the immersed boundary method [27], the front tracking method [37, 35], the level set method [33, 30, 26], and the volume-of-fluid method [28, 15]. To deal with the singular source term $F(x, t)$ such as the surface tension in equation (1), these methods simply use a discrete delta function to transform the source term $F(x, t)$ defined only on the interface to the grid cells near the interface, and then solve the Navier-Stokes equations as a one-phase problem.

Recently, sharp interface methods to solve the two-phase flows directly using the jump conditions due to the singular force term have received attention. The ghost-fluid method [12, 22, 16] has been used to solve the elliptic boundary value/elliptic interface problem, and then used to solve the two-phase incompressible flow to more accurately compute the solution satisfying the jump conditions for the Navier-Stokes equations across the material interface. However, since the ghost-fluid method uses approximate jump conditions, it can only achieve at most first order accuracy for the elliptic interface problem. Another popular method is the immersed interface method [19, 20, 18, 34] which has been applied to solve elliptic interface problems, parabolic interface problems, and two-phase incompressible flow with discontinuous viscosity. However, it seems that this method has not been used to solve variable density two-phase incompressible flow. In addition to the basic jump conditions, the immersed interface method requires higher-order derivative jump conditions, which are often difficult to be derived.

In this paper, we develop an embedded boundary method (EBM) [14] to solve the two-phase incompressible Navier-Stokes equations with piecewise constant density. This method was originally proposed [14] to solve the elliptic boundary value problem on irregular domains. It has since been used to solve the heat equation [24, 29] and the incompressible flow on a time-dependent domain [25] with second order accuracy. Recently it has been extended to solve the elliptic interface problem with second order accuracy in two and three dimension [39, 8] where the jump conditions for the potential and its flux are used in the discretization of the elliptic equations using the finite volume method.

The front tracking code `FRONTIER` developed at Stony Brook University has been successfully used for solving compressible flow [11, 9, 5]. It uses the ghost-fluid method [12, 22, 16] to obtain sharp interface solution. In this paper, we solve the two-phase incompressible flow equations using the embedded boundary method, with the front tracking method used to track the material interface. The jump conditions due to the surface tension force are accurately solved in the projection step using the EBM while the jump conditions due to the discontinuous viscosity are disregarded for simplicity. The main contribution of this paper is the development of a sharp interface EBM for the two phase incompressible flow. We also demonstrate the extension of the method to the cylindrical coordinate. An extension of the method has been used to solve large density ratio incompressible multiphase magnetohydrodynamic flows [1].

The paper is organized as follows. In section 2, we review briefly the projection method used to solve the incompressible flow without considering the interface. In section 3, we describe the embedded boundary method used to solve the incompressible flow with an internal interface. In section 4, we show some examples to verify our methods. Finally, we give the conclusion. In the appendices, we discuss the consequence of not considering the jump condition due to discontinuous viscosity, the code structure, and parallelization.

2 The Projection Method

In this section, we give the basic description of the projection methods used to solve the incompressible flow without considering the interface. Zhou et al. [40] presented the verification of the basic code for solving one phase flow and an implementation of the two phase flow using the immersed boundary method with the front tracking method.

To solve the Navier-Stokes equation, one of the most popular methods is the projection method. There are many variations of the projection method [6]. In this paper, we use two different but similar projection methods (denoted as PM1 and PM3 later on) with the embedded boundary method to solve the two-phase incompressible flow (PM1 is first order accurate and PM2 is second order accurate when there is no interface). The projection methods for solving the Navier-Stokes equations (1) consists of two steps [6]. The first step solves the convection and diffusion term to compute an intermediate velocity at the new time step. The second step then solves the Poisson equation to obtain the pressure, and use the new pressure to calculate the new time step velocity, which satisfies the divergence free condition. One salient feature of the two projection methods used in this paper is that the pressure instead of the pressure increment is calculated in the projection step. This feature makes it easier to use the EBM. The reason is that for two phase incompressible flow with surface tension, it is the pressure (not the pressure increment) which has a jump equal to the surface tension across the interface.

2.1 Projection Methods

We describe three different variations of the projection methods. However, the last projection method (denoted as PM3 later on) is presented here only for comparison purpose and is not used in our algorithms. For simplicity, we use L to denote the discretization of the heat operator in the Navier-Stokes equations.

2.1.1 Projection Method PM1

This projection method is similar to Chorin's original projection method [7, 6].

$$u^* = L(u^n, -u \cdot \nabla u)$$

$$\frac{u^{n+1} - u^*}{\Delta t} = -\frac{1}{\rho} \nabla p^{n+\frac{1}{2}} \quad (2)$$

where n is the time step index, Δt is the time step size, u^* is the intermediate velocity, and u^{n+1} is the velocity at the new time step satisfying the divergence free property. Note that this method is only first order accurate. A notable characteristics of this method is that the projection step solves for the pressure $p^{n+\frac{1}{2}}$ instead of the pressure increment.

2.1.2 Projection Method PM2

A second order accurate method [25] is the following

$$\tilde{u} = L(u^n, -u \cdot \nabla u, -\nabla p^{n-\frac{1}{2}}) \quad (3)$$

$$\frac{u^* - \tilde{u}}{\Delta t} = \frac{1}{\rho} \nabla p^{n-\frac{1}{2}} \quad (4)$$

$$\frac{u^{n+1} - u^*}{\Delta t} = -\frac{1}{\rho} \nabla p^{n+\frac{1}{2}} \quad (5)$$

This method has the same property as PM1 in that the projection step solves for the pressure $p^{n+\frac{1}{2}}$ instead of the pressure increment. This makes it easy to use our EBM method when a jump condition about the pressure (instead of pressure increment) is given.

2.1.3 Projection Method PM3

Another popular second order accurate method is given by Bell, et al [3, 6]:

$$u^* = L(u^n, -u \cdot \nabla u, -\nabla p^{n-\frac{1}{2}})$$

$$\frac{u^{n+1} - u^*}{\Delta t} = -\frac{1}{\rho} \nabla \phi^{n+\frac{1}{2}} \quad (6)$$

$$p^{n+\frac{1}{2}} = p^{n-\frac{1}{2}} + \phi^{n+\frac{1}{2}}$$

Note that the projection step solves for the pressure increment $\phi^{n+\frac{1}{2}}$. For this reason, it is difficult to be used with a jump condition for the pressure itself (such as the surface tension between two phases). Thus, this method is not used in this paper.

2.2 Time Discretization for the Calculation of the Intermediate Velocity

There are many different methods to discretize the heat operator. In the following, we briefly describe the Crank-Nicolson method and the Additive Runge-Kutta Method that we have used in our method.

2.2.1 Crank-Nicolson Method

Using the Crank-Nicolson method for the heat operator and using PM1 as example, we have

$$\rho \left(\frac{u^* - u^n}{\Delta t} \right) = -(u \cdot \nabla) u^{n+\frac{1}{2}} + \frac{1}{2} (\mu \nabla^2 u^* + \mu \nabla^2 u^n) + g \quad (7)$$

where the convection term is solved using an explicit Godunov-type scheme as in [4]:

Table 1: Additive Runge-Kutta coefficients tableau

c_1	a_{11}	...	a_{1s}	b_{11}	...	b_{1s}
...
c_s	a_{s1}	...	a_{ss}	b_{s1}	...	b_{ss}

- extrapolate the velocity to the cell face at time $n + \frac{1}{2}$ (the following shows the formula for only one face):

$$u_{i+1/2,j}^{n+1/2} = u_{i,j}^n + \frac{1}{2}\Delta x \left. \frac{\partial u}{\partial x} \right|_{i,j}^n + \frac{1}{2}\Delta t \left. \frac{\partial u}{\partial t} \right|_{i,j}^n, \quad (8)$$

where i, j denote the cell index, $(i+1/2, j)$ denotes one of the the cell face, n denote the time step index, and $\frac{\partial u}{\partial t}$ can be replaced by the Navier-Stokes equations

$$u_t = -(u \cdot \nabla)u - \frac{1}{\rho}\nabla p + \mu(\nabla^2 u) + g(x, t).$$

- solve the Riemann problem (Burgers' equation) to find the cell face velocity at time $n + \frac{1}{2}$.
- use the cell face velocity to calculate the convection term $(u \cdot \nabla u)^{n+\frac{1}{2}}$.

2.2.2 Additive Runge-Kutta Method

The implicit Runge-Kutta method ([36]) was used to solve the time dependent parabolic initial boundary value problem in ([24, 29]) and the parabolic interface problem in [39]. In this paper, we instead use the additive Runge-Kutta method [21] which seems to be easier for the discretization of the Navier-Stokes equation.

Using the notation in [21], we want to solve the following ordinary differential equation (ODE):

$$y'(t) = f(t, y) + g(t, y) \quad (9)$$

where f is linear operator of y and g is a nonlinear operator. We use an implicit scheme for f and an explicit scheme for g . When used with PM2, $f = \Delta u$ and $g = -u \cdot \nabla u - \nabla p^{n-\frac{1}{2}}$. Note that to solve the convection term $u \cdot \nabla u$ for the additive Runge-Kutta method, there is no need to do time extrapolation in equation (8).

To solve the ODE (9), the s -stage Runge-Kutta method has the following form

$$y_i^{(n)} = y_s^{(n-1)} + h \sum_{j=1}^s a_{ij} f(t_{n-1} + c_j h, y_j^{(n)}) + h \sum_{j=1}^s b_{ij} g(t_{n-1} + c_j h, y_j^{(n)})$$

where $i = 1, 2, \dots, s$, $n = 1, 2, 3, \dots$, and $c_i = \sum_{j=1}^s a_{ij} = \sum_{j=1}^s b_{ij}$. The coefficients are generally written as the tableau in Table 1.

In this paper, we use the L -stable two stage additive Runge-Kutta scheme shown in Table 2.

Table 2: L-stable two stage additive scheme

0	0	0	0	0	0	0
$\frac{1}{2}$	$\frac{1}{2}(-1 + \sqrt{2})$	$1 - \frac{\sqrt{2}}{2}$	0	$\frac{1}{2}$	0	0
1	$1 - \frac{\sqrt{2}}{2}$	$\sqrt{2}-1$	$1 - \frac{\sqrt{2}}{2}$	0	1	0

2.3 Calculation of the New Velocity

Now we consider the projection step of PM1 and PM2 for calculating the pressure and the new divergence free velocity. For a regular grid cell containing no interface, the new velocity is calculated using:

$$\rho \left(\frac{u^{n+1} - u^*}{\Delta t} \right) = -\nabla p^{n+1/2} \quad (10)$$

where $p^{n+1/2}$ denotes the new pressure and is calculated using

$$\nabla \cdot \left(\frac{1}{\rho} \nabla p^{n+1/2} \right) = \frac{1}{\Delta t} \nabla \cdot u^*, \quad (11)$$

and the boundary condition

$$n \cdot \nabla p^{n+1/2} = 0. \quad (12)$$

We have used $\nabla \cdot u^{n+1} = 0$ and equation (10) to obtain the Poisson equation (11).

3 The EBM for Two-Phase Incompressible Flow

In this section, we first review the jump conditions of the incompressible flow with an internal interface. Next we review our embedded boundary method for solving the elliptic interface problem in subsection 3.2. Then we show how to use the EBM in a cylindrical coordinate system. The method to calculate the pressure gradient used in PM2 is described in subsection 3.4. At last we apply the EBM to solve the elliptic interface problem of the projection step for the two-phase incompressible flow in subsection 3.5.

3.1 The Jump Conditions across an Internal Interface

For two phase flow with discontinuous coefficients, the solutions satisfy the following jump conditions across the internal interface:

$$[u] = 0 \quad (13)$$

$$[p] = 2[\mu \frac{\partial u}{\partial n}] \cdot n + f \cdot n \quad (14)$$

$$[\mu \frac{\partial u}{\partial n}] \cdot \tau + [\mu \frac{\partial u}{\partial \tau}] \cdot n + f \cdot \tau = 0 \quad (15)$$

$$[\frac{\partial u}{\partial n}] \cdot n = 0 \quad (16)$$

$$[\frac{1}{\rho} \frac{\partial p}{\partial n}] = 0 \quad (17)$$

where n is the normal vector and τ is the tangential vector. Note that we have four jump conditions for the two velocity components in $2D$ (six in $3D$) and two jump conditions for the pressure.

- Jump condition (13) is due to the viscous flow (Zhi, et al [34]).
- Jump conditions (14, 15) are the result of force balancing in the normal and tangential directions (Ito and Li [13]). The derivation of the jump conditions (14,15) is given by Ito and Li [13] for the Stokes equations. It is trivial to extend it for Navier-Stokes equation.
- Jump condition (16) is due to $[\nabla \cdot u] = 0$ (Lai and Li [17]).
- Jump condition (17) is needed to obtain a continuous velocity in the normal direction across the interface when solving the elliptic interface problem for the pressure.

In this paper, we assume that the singular force term on the interface has only a normal component, which means that $f \cdot \tau = 0$. The surface tension force satisfies this assumption. For simplicity, we also ignore the jump conditions due to the discontinuous viscosity. Appendix A shows the consequence of such a simplification. Therefore the velocity and its derivatives are continuous across the interface, while the pressure has a jump equal to the surface tension across the interface.

3.2 The Embedded Boundary Method for the Elliptic Interface Problem

We review briefly the embedded boundary method for solving the elliptic interface problem. For more detail, refer to [39, 8, 14, 24]. We assume that the interface can only cross any cell edge at most once, as implicitly assumed in the Marching Cubes algorithm [23]. This assumption is necessary to limit the number of different cases that could arise. The geometric information needed of the partial cells needed by the embedded boundary method is calculated using the divergence theorem for each cell case by case [38].

The elliptic interface problem is a special elliptic problem with an internal interface:

$$\nabla \cdot \frac{\nabla p}{\rho} = f \quad (18)$$

Table 3: Number of material components and cell unknowns for different cell types

Cell Type	Number of		
	Components	Center Unknowns	Interface Unknowns
External	N/A	N/A	N/A
Internal	1	1	0
Boundary	1	1	0
Partial	2	2	2

where ρ is a piecewise continuous function with jump across the internal interface and f is a given function which is continuous inside each part of the domain. To close the problem, boundary conditions are needed for the exterior and interior boundary. Either Dirichlet or Neumann boundary can be given on the exterior boundary. For the interior interface, we have the following two jump conditions:

$$[p] = J_1(\mathbf{x}), \quad (19)$$

$$\left[\frac{1}{\rho} \frac{\partial p}{\partial n}\right] = J_2(\mathbf{x}), \quad (20)$$

where J_1 and J_2 are given functions of the spatial variables [19]. Note that our method could be easily extended to more general cases where J_1 and J_2 are functions of the unknown variables p defined on the interface.

The EBM can be used to solve the elliptic problem with an irregular domain boundary and an internal interface. It uses a Cartesian mesh. The mesh cells are classified into four types:

- An *external* cell is outside of the computational domain and thus is not used in the computation.
- An *internal* cell is a cell wholly located inside the computational domain, possibly with one of its cell face being the domain boundary.
- A *boundary* cell is a cell intersected by the irregular exterior domain boundary with part of the cell out of the domain and part of the cell inside the domain.
- A *partial* cell is a cell intersected by the internal interface. It is separated into two or more parts by the internal interface. Those different parts are also called partial cells in the following.

When the EBM is used to solve the elliptic interface problem, one or more unknowns are defined at the cell center, as shown in Table 3. For an interior cell or a boundary cell, only one unknown is needed at the cell center and a standard finite volume method can be used to setup one algebraic equation using the elliptic equation as in [39, 14, 24, 29]. For a partial cell, four unknowns in total are needed to make the discretization of the elliptic equation consistent with

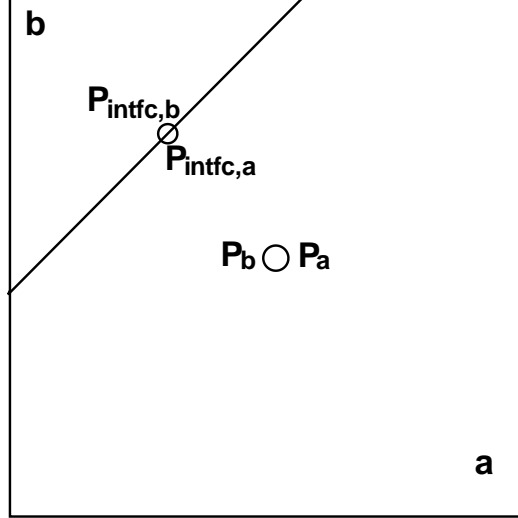


Figure 1: Placement of unknowns in a partial cell containing the cell internal interface. p_a and p_b are cell center unknowns for component a and b respectively. Similarly, $p_{intfc,a}$ and $p_{intfc,b}$ are cell interface unknowns for component a and b respectively.

the two interface jump conditions (19), (20). Figure 1 depicts the placement of unknowns in a partial cell with internal interface. The cell contains two partial cells (for material components a and b) which are separated by the interface. For each partial cell, there is one unknown defined at the cell center (p_a for component a , p_b for component b) for the discretization of the elliptic equation. In order to satisfy the two jump conditions (19, 20), two more unknowns $p_{intfc,a}$ and $p_{intfc,b}$ are defined at the center of the cell internal interface (portion of the interface contained within the cell) for the two components a and b . Thus, four unknowns are defined in total for one partial cell. Four algebraic equations can be constructed using the elliptic equation for the two partial cells and the two jump conditions across the cell internal interface

3.2.1 Discretization of the Jump Conditions

We first describe the method for the discretization of the two jump conditions across the interface for the cell (i, j) . A schematic of the corresponding stencil and states used in the interpolation method is shown in Figure 2. Two unknowns $p_{intfc,a}$ and $p_{intfc,b}$ are defined at the center of the cell interface for components a and b respectively.

We assume the direction of the normal to the interface as pointing from a

the polynomial. Denoting the coordinate locations of the unknowns as (x_1, y_1) , (x_2, y_2) , and (x_3, y_3) , the unknowns as p_1 , p_2 , and p_3 , we have

$$\begin{pmatrix} 1 & x_1 & y_1 \\ 1 & x_2 & y_2 \\ 1 & x_3 & y_3 \end{pmatrix} \begin{pmatrix} \beta_0 \\ \beta_1 \\ \beta_2 \end{pmatrix} = \begin{pmatrix} p_1 \\ p_2 \\ p_3 \end{pmatrix}.$$

Denoting the above matrix as X , the coefficient vector as β , and the right hand side as P , we have

$$X\beta = P,$$

or

$$\beta = X^{-1}P.$$

Now the constructed polynomial can be written as

$$(1 \ x \ y) \begin{pmatrix} \beta_0 \\ \beta_1 \\ \beta_2 \end{pmatrix}.$$

The derivatives of the polynomial can be written as

$$\begin{aligned} p_x &= \beta_1 \\ p_y &= \beta_2 \\ \frac{\partial p}{\partial n} &= p_x n_1 + p_y n_2 = (0 \ n_1 \ n_2) \begin{pmatrix} \beta_0 \\ \beta_1 \\ \beta_2 \end{pmatrix} = \hat{n}^T \beta \end{aligned} \quad (23)$$

where $n = (n_1, n_2)^T$ is the unit normal vector, and $\hat{n} = (0, n_1, n_2)^T$. Thus we have

$$\begin{aligned} \frac{\partial p}{\partial n} &= \hat{n}^T X^{-1}P \\ &= ((X^{-1})^T \hat{n})^T P, \\ &= ((X^T)^{-1} \hat{n})^T P \end{aligned}$$

Therefore, we can represent $\frac{\partial p}{\partial n}$ as a linear combination of the unknowns P . Similarly, we can calculate the directional derivative using second degree polynomial construction.

Now suppose that instead we want to use least square fitting, we have

$$\beta = ((X^T X)^{-1} X^T)P.$$

The directional derivative can be calculated as

$$\begin{aligned} \frac{\partial p}{\partial n} &= \hat{n}^T \beta = \hat{n}^T ((X^T X)^{-1} X^T)P \\ &= (X(X^T X)^{-1} \hat{n})^T P, \end{aligned}$$

thus $\frac{\partial p}{\partial n}$ can also be written as a linear combination of the unknowns P .

3.2.2 Equations for the Cell Center Unknowns

For the two cell center unknowns defined at the partial cell (i, j) , we can use the EBM technique to set up two algebraic equations by integrating the elliptic equation over the corresponding partial cells. See Figure 2 for the stencil to set up the equation for the unknown of the component a using the partial cell $cdef$.

Integrating the equation (18) over the partial cell $cdef$ and using the divergence theorem, we obtain the following expressions:

$$\iint_{cdef} \nabla \cdot \frac{\nabla p}{\rho} dx dy = \oint_{\partial(cdef)} \frac{\nabla p}{\rho} \cdot nds = \iint_{cdef} f dx dy,$$

or

$$\int_{cd} \frac{\nabla p}{\rho} \cdot nds + \int_{de} \frac{\nabla p}{\rho} \cdot nds + \int_{ef} \frac{\nabla p}{\rho} \cdot nds + \int_{fc} \frac{\nabla p}{\rho} \cdot nds = \iint_{cdef} f dx dy,$$

which is

$$l_{cd} \cdot flux_{cd} + l_{de} \cdot flux_{de} + l_{ef} \cdot flux_{ef} + l_{fc} \cdot flux_{fc} = \iint_{cdef} f dx dy \quad (24)$$

where l_{mn} is the length between m and n . Therefore we only need to calculate the flux across the cell edges or cell interface. For $flux_{cd}$, a second order derivative is calculated by using a linear interpolation of $\frac{p_{i,j-1}-p_{i,j}}{\Delta x}$ and $\frac{p_{i+1,j-1}-p_{i+1,j}}{\Delta x}$ to the center of cd (see [39, 14]). For $flux_{de}$, we simply use $\frac{p_{i+1,j}-p_{i,j}}{\Delta y}$ to calculate the derivative. For $flux_{ef}$, a linear interpolation of $\frac{p_{i,j+1}-p_{i,j}}{\Delta x}$ and $\frac{p_{i+1,j+1}-p_{i+1,j}}{\Delta x}$ to the center of ef is used. And $flux_{fc}$ is calculated by $\frac{\partial p}{\partial n}|_a$ used in (22). Note that we need to multiply the derivatives calculated with $\frac{1}{\rho}$ at the corresponding edge or cell interface center to obtain the flux. In the same way, we calculate fluxes for the other partial cells. More details can be found in [39, 14].

3.2.3 Geometric Property Calculation

We use 3D as example. Since the EBM is a finite volume method, we need to calculate the partial cell volumes accurately. To solve the elliptic interface problem, we also need to calculate the cell interface area, normal and center.

Due to the assumption that the interface crosses the cell edge at most once, there are finite number of cases for the partial cell configurations with two components. The cell volume, cell interface area, interface normal, and interface center are calculated case by case by using the divergence theorem:

$$\int_{\Omega} \nabla \cdot F dv = \int_{\partial\Omega} \vec{n} \cdot F ds. \quad (25)$$

where $\vec{F} = (F_x, F_y, F_z)$. Thus, we can use a cell boundary integration instead of a cell volume integration to calculate the geometric information needed.

In the Cartesian coordinate, the divergence operator is defined as

$$\nabla \cdot \vec{F} = \frac{\partial F_x}{\partial x} + \frac{\partial F_y}{\partial y} + \frac{\partial F_z}{\partial z}.$$

To calculate the volume of the domain Ω , we can let $\vec{F} = \vec{X} = (x, y, z)^T$ where \vec{X} is the Cartesian coordinate. Note that F is not unique. Then we have

$$\begin{aligned} \int_{\Omega} \nabla \cdot \vec{F} dv &= \int_{\partial\Omega} n \cdot \vec{F} ds \\ \int_{\Omega} 3dv &= \int_{\partial\Omega} n \cdot \vec{X} ds \end{aligned}$$

Therefore, we can calculate the volume using the surface integration

$$Volume = \int_{\Omega} dv = \frac{\int_{\partial\Omega} n \cdot \vec{X} ds}{3}. \quad (26)$$

For the cell interface area, normal and center, we do surface integrations:

$$\begin{aligned} &\int_{intfc} ds \\ &\int_{intfc} \vec{n} ds \\ &\int_{intfc} \vec{X} ds \end{aligned}$$

where *intfc* refers to the cell interface. For more detail, refer to [38].

3.3 The Embedded Boundary Method in Cylindrical Coordinates

In this subsection, we briefly describe the embedded boundary method used to solve an elliptic interface problem in a cylindrical coordinate.

To discretize the elliptic equation (18) for a mesh cell, we use the divergence theorem to get

$$\oint \frac{\nabla p}{\rho} \cdot n ds = \int f dv$$

or

$$\oint \frac{1}{\rho} \frac{\partial p}{\partial n} ds = \int f dv$$

This is true for all coordinate systems. However, we need to change the formula for the calculation of the geometric property for the mesh cell, such as the cell face area, cell volume, cell interface area, normal and the center. The formula for the flux calculations across the cell face and the cell internal interface also need to be modified.

3.3.1 Finite Difference Scheme for the Flux Calculation

To calculate the flux across the cell faces or partial cell interface, we use

$$\frac{\partial p}{\partial n} = \nabla p \cdot \vec{n}$$

where the gradient operator is defined as

$$\nabla = \vec{r} \frac{\partial}{\partial r} + \vec{\theta} \frac{1}{r} \frac{\partial}{\partial \theta} + \vec{z} \frac{\partial}{\partial z}$$

and \vec{n} is the normal of the cell faces.

For the flux across the partial cell interface, we need to modify the equation 23 using the Cylindrical coordinate directional derivative instead.

3.3.2 Geometric Property Calculation

The surface elements in cylindrical coordinate for the cell face of the internal cell are

$$\begin{aligned} ds &= rd\theta dz, \\ ds &= dr dz, \\ ds &= r dr d\theta \end{aligned}$$

in the respective coordinate planes. They can be used to calculate the cell face area for the 6 cell faces. The volume element is

$$dv = r dr d\theta dz.$$

To calculate the partial cell volume, we also use the divergence theorem. In a cylindrical coordinate, the divergence operator is defined as

$$\nabla \cdot \vec{F} = \frac{1}{r} \frac{\partial}{\partial r}(rF_r) + \frac{1}{r} \frac{\partial F_\theta}{\partial \theta} + \frac{\partial F_z}{\partial z}.$$

To calculate the volume of the domain Ω , we can let $\vec{F} = (r, r\theta, z)^T$, and then we have

$$\begin{aligned} \int_{\Omega} \nabla \cdot \vec{F} dv &= \int_{\partial\Omega} n \cdot \vec{F} ds \\ \int_{\Omega} 4dv &= \int_{\partial\Omega} n \cdot \vec{F} ds \end{aligned}$$

Note that the choice for \vec{F} is not unique. Therefore, we can calculate the volume using the surface integration

$$Volume = \int_{\Omega} dv = \frac{\int_{\partial\Omega} n \cdot \vec{F} ds}{4}. \quad (27)$$

For more detail, refer to [38].

3.4 Calculation of the Pressure Gradient

To calculate the pressure gradient used in (3) and (4), we simply use least square fitting. To calculate the gradient for cell (i, j) with component c , we do the following:

1. find the nearest cell (\hat{i}, \hat{j}) containing component c .
2. collect all the states with the same component from neighboring cells with cell index (\tilde{i}, \tilde{j}) satisfying $|\tilde{i} - \hat{i}| \leq 2$ and $|\tilde{j} - \hat{j}| \leq 2$.
3. use least square fitting to fit a quadratic polynomial and take gradient to calculate the pressure gradient needed. See subsection 3.2.1 for detail.

3.5 The EBM for the Projection Step

We solve the elliptic equation (11) in the projection step. The EBM for a general elliptic interface problem is given in previous subsections. The two jump conditions given by (14, 17) are used to connect the pressure solution across the interface.

Thus, for the projection step, the equation is

$$\nabla \cdot \left(\frac{1}{\rho} \nabla (p^{n+1/2}) \right) = \frac{1}{\Delta t} \nabla \cdot u^* \quad (28)$$

coupled with the two jump conditions (omitting the effect due to the viscosity jump across the interface)

$$[p^{n+1/2}] = f \cdot n \quad (29)$$

and

$$\left[\frac{1}{\rho} \frac{\partial p^{n+1/2}}{\partial n} \right] = 0 \quad (30)$$

where $f \cdot n = \sigma \kappa$ for the surface tension force between the two phases (σ is the surface tension coefficient and κ is the mean curvature).

Our projection method consists of the following steps:

1. Calculate cell face velocity u_{face}^* using intermediate cell center velocity u^* by linear interpolation.
2. Calculate the elliptic interface equation for p :

$$\begin{cases} \nabla \cdot \frac{\nabla p}{\rho} = \frac{1}{\Delta t} \nabla \cdot u_{face}^* \\ [p] = \sigma \kappa \\ \left[\frac{1}{\rho} \frac{\partial p}{\partial n} \right] = 0 \end{cases}$$

where the right hand side of the elliptic equation is calculated using the divergence theorem.

3. Calculate the projected cell face velocity $u_{face,c}^{n+1}$ for each full/partial cell face using:

$$u_{face,c}^{n+1} = u_{face}^* - \frac{\Delta t}{\rho_{face,c}} \cdot \frac{\partial p}{\partial n} \Big|_{face,c}$$

where $\nabla p_{face,c}$ is calculated using the cell center pressure for component c .

4. Calculate the averaged cell face velocity u_{face}^{n+1} using $u_{face,c}^{n+1}$. For example, in Figure 2,

$$u_{ge}^{n+1} = \frac{l_{gf}u_{gf,b}^{n+1} + l_{fe}u_{fe,a}^{n+1}}{l_{ge}}$$

where l_{ge} , l_{fg} , l_{fe} are the length between corresponding point on the cell face, $u_{gf,b}^{n+1}$ is the velocity through gf and $u_{fe,a}^{n+1}$ is the velocity through fe .

5. Calculate the cell centered velocity using u_{face}^{n+1} by using the 2nd order TVD reconstruction algorithms [2]. A simple alternative is to use interpolation of the cell face velocity to calculate the cell center velocity.

4 Examples

We compare theoretical and simulated bubble oscillation frequencies in $2D$ and $3D$ to verify our embedded boundary method to solve two-phase incompressible flow. To apply EBM to cylindrical coordinates, we first verify the accuracy of the EBM by solving an elliptic interface problem with known solution. Then we apply our methods to solve a more complicated problem of engineering interest.

4.1 Bubble Oscillation in Two and Three Dimension

We consider the oscillation period of a droplet under zero gravity, for which there is an analytical solution and the surface tension is the dominant force. We have used both PM1 and PM2 to obtain the simulation result. However, it is found that the difference between the results obtained using the two methods are negligible.

4.1.1 Bubble Oscillation in Two Dimension

For a $2D$ droplet under zero gravity, when the initial position of the droplet interface with small perturbation is given by

$$R(\theta) = R_0 + \epsilon \cos(n\theta)$$

where R_0 the unperturbed radius, ϵ is the amplitude of the perturbation and n is the order of the Legendre polynomial, the oscillation frequency is given in [10, 31] as

$$\omega_n = \sqrt{\frac{(n^3 - n)\sigma}{(\rho_d + \rho_o)R_0^3}}$$

Table 4: Bubble Oscillation in 2D, domain $[0, 2] \times [0, 2]$, $\rho = \{1, 0.05\}$, $\nu = \{0.0005, 0.0005 \times 0.01\}$, $\sigma = 0.5$, $R_0 = 0.8$, $n = 2$ and $\epsilon = 0.05$. with theoretical period $T_2 = 2.56638189$

Mesh Size	Period	Error in Percentage
20x20	3.4602	17.45
40x40	3.0476	9.95
80x80	2.8962	6.38
160x160	2.7643	3.93

where ρ_d and ρ_o are the densities for the droplet and outer fluid and σ is the surface tension coefficient.

The period is given by

$$T_n = \frac{2\pi}{\omega_n}.$$

We run the simulation with the domain as $[0, 2] \times [0, 2]$, the densities and dynamic viscosities of the droplet and the outer fluid given by $\rho = \{1, 0.05\}$, $\nu = \{0.0005, 0.0005 \times 0.01\}$. We impose a surface tension coefficient of $\sigma = 0.5$. For the initial interfacial position, we use $R_0 = 0.8$, $n = 2$ and $\epsilon = 0.05$. Table 4 shows the convergence of the oscillation period under mesh refinement. Figure 3 shows the interface velocity of the droplet at time $t = 0.5$. From the picture we can see that the interface velocity changes smoothly along the interface. Figure 4 shows the pressure over the whole computational domain. It is apparent that the pressure has a jump across the interface due to the surface tension. Due to the small perturbation of the initial interface ($\epsilon = 0.05$) and large radius of the droplet ($R_0 = 0.8$), the variation of the surface tension along the interface is very small. Therefore, the variation of the pressure jump along the interface is small and not apparent in the figure. We observe the accurate resolution of the pressure discontinuity up to the interface without over shoots, the Gibbs phenomenon.

4.1.2 Bubble Oscillation in Three Dimension

For a 3D droplet under zero-gravity, when the initial position of the droplet interface with small perturbation [32] is given by

$$r(\theta, t) = R_0 + \epsilon P_n(\cos(\theta)),$$

where R_0 is the radius of the droplet, P_n is the Legendre polynomial of order n , ϵ is the amplitude of the perturbation, then the frequency of the droplet oscillation is given by

$$\omega_n = \sqrt{\frac{1}{We} \frac{n(n-1)(n+1)(n+2)}{R_0^3(n+1+n\lambda)}}$$

where $\lambda = \frac{\rho_d}{\rho_o}$, and $We = \frac{\rho_l U^2}{\sigma}$ is the Weber number.

Figure 3: Bubble Oscillation in $2D$, with interface velocity drawn as vector starting from the interface at time $t = 0.5$

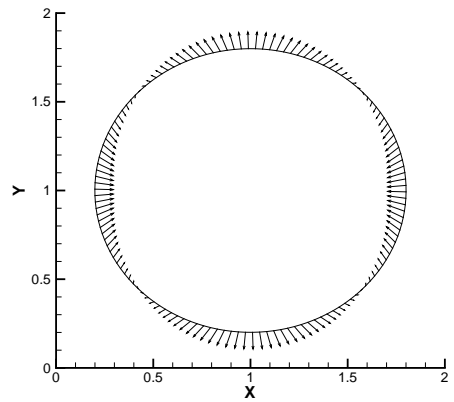


Figure 4: Bubble Oscillation in $2D$, Pressure at time $t = 0.5$

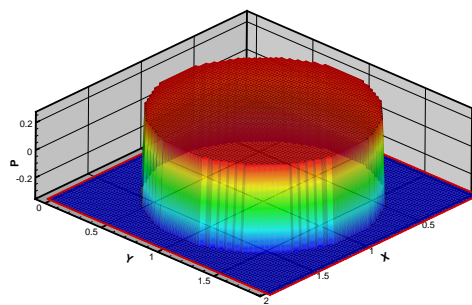
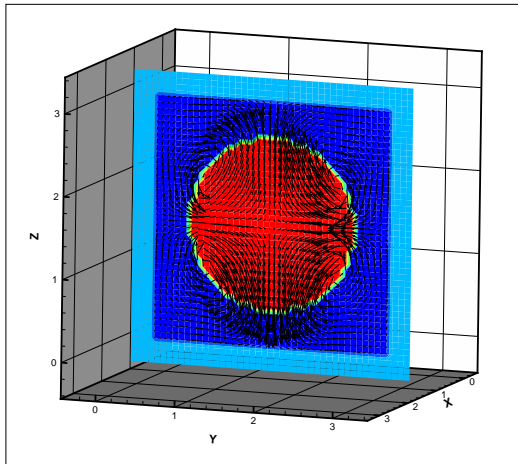


Table 5: Bubble Oscillation in 3D, theoretical period is $T_2 = 2.222$

Mesh Size	Period	Error in Percentage
20x20x20	2.433	9.5%
40x40x40	2.300	3.5%
80x80x80	2.184	1.71%

Figure 5: Bubble Oscillation in 3D, Velocity Field on a Slice through the Center of the Droplet at $t = 1.8$



We perform the 3D simulation with the domain as $[0, 3] \times [0, 3] \times [0, 3]$. We use $Re = \frac{\rho_l LU}{\mu_l} = 2000$, $We = \frac{\rho_l LU^2}{\sigma} = 1$ and $\rho_d = 1$, $\rho_o = 0.001$, $\mu_d = 0.0005$, $\mu_o = 0.000005$. Table 5 shows the convergence of the oscillation period under mesh refinement. Figure 5 shows the velocity field on a slice through the center of the droplet.

4.2 EBM for the Elliptic Interface Problem in Cylindrical Coordinates

We use the method of manufactured solutions to verify our EBM implementation for the elliptic interface problem in the cylindrical coordinates. The computational domain is $r \in [1, 1.628]$, $\theta \in [0, 0.628]$ and $z \in [0, 0.628]$. The interface position is a sphere relative to the cylindrical coordinates, given as

$$\sqrt{(r - 1.314)^2 + (\theta - 0.314)^2 + (z - 0.314)^2} = 0.2.$$

We use $\rho_d = 0.811$ for the density inside the sphere and $\rho_o = 1.03$ for the density outside. We solve the equation

$$\nabla \cdot \frac{\nabla p}{\rho} = f \tag{31}$$

Table 6: Mesh Convergence Study for the Elliptic Interface Problem in Cylindrical Coordinates

Mesh Size	L_∞ Error	L_2 Error	L_1 Error
10x10x10	0.00018217	0.00002381	0.00004517
20x20x20	0.00009903	0.00000659	0.00001244
40x40x40	0.00001539	0.00000174	0.00000327
80x80x80	0.00000415	0.00000045	0.00000084

where f is a given function. We use

$$p(r, \theta, z) = e^{-\frac{r^2 + \theta^2 + z^2}{5}}$$

as the exact solution and substitute into the elliptic equation (31) to calculate the right hand side f . Table 6 shows the mesh convergence for the this problem. From the table, we can see that the method is second order accurate.

4.3 High Speed Two Phase Couette Flow

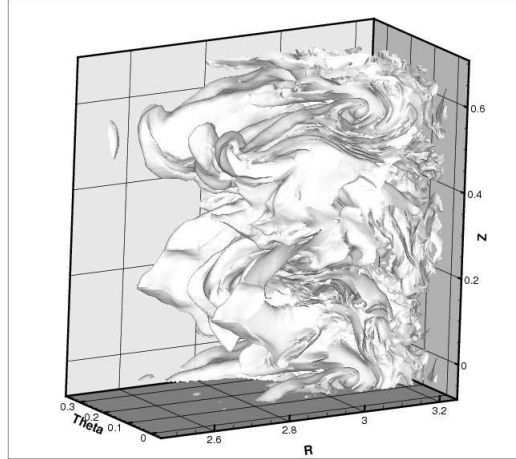
Here we use the EBM to simulate high speed two-phase Couette mixing in a 3D angular sector. A more detailed description of this simulation using the immersed boundary method can be found in [40]. In the current simulation, we use $\rho_{aqu} = 1.03g/cm^3$ and $\rho_{org} = 0.811g/cm^3$ for the fluid densities for the aqueous and organic phase respectively, $\mu_{aqu} = 0.0102g/cm \cdot s$ and $\mu_{org} = 0.016g/cm \cdot s$ for the viscosities, and $\sigma = 10dyn/cm$ for the surface tension. The computational domain is an angular sector of the cylinder with $r \in [2.538, 3.166]$, $\theta \in [0, 0.314]$, $z \in [0, 0.628]$. Figure 6 shows the interface position at $t = 28\mu s$.

The explanation of the result will be given in another paper. This example is given here to show the capability of the implemented EBM to deal with problem with complex interface and of engineering interest. Under the assumption that there is at most one interface crossing on each cell edge, there are $2^8 = 256$ possible cases for a mesh cell. The numerical simulation results for this example show that all 256 cases appeared at the same time.

5 Conclusions

In this paper, we extended the embedded boundary method to solve the two-phase incompressible flow. We verify our method by solving the droplet oscillation problems in 2D and 3D. We also show that the EBM can be easily extended to solve the elliptic interface problem in other coordinate systems such as the cylindrical coordinates. Finally, we simulated the interface contact problem in a rotating cylinder to show the robustness of the method. Currently, we did not consider the jump condition due to the discontinuous viscosity. This will be addressed in the future.

Figure 6: Interface for Two Phase Couette Flow



6 Acknowledgment

This work is supported in part by Army Research Office W911NF0910306. Computational resources were provided by the Stony Brook Galaxy cluster, the Stony Brook/BNL New York Blue Gene/L IBM machine.

References

- [1] *Sharp Interface Algorithm for Large Density Ratio Incompressible Multiphase Magnetohydrodynamic Flows*. Elsevier, 2013.
- [2] Dinshaw S. Balsara. Divergence-free adaptive mesh refinement for magnetohydrodynamics. *J. Comput. Phys.*, 174:614–648, 2001.
- [3] J. B. Bell, P. Colella, and H. M. Glaz. A second order projection method for the incompressible Navier-Stokes equations. *J. Comput. Phys.*, 85:257, 1989.
- [4] J. B. Bell, P. Colella, and H. M. Glaz. A second order projection method for the incompressible navier-stokes equations. *J. Comput. Phys.*, 85:257, 1989.
- [5] W. Bo, X. Liu, J. Glimm, and X. Li. A robust front tracking method: Verification and application to simulation of the primary breakup of a liquid jet. *SIAM J. Sci. Comput.*, 33(4):1505–1524, 2011.
- [6] David L. Brown, Ricardo Cortez, and Michael L. Minion. Accurate projection methods for the incompressible navier-stokes equations. *J. Comput. Phys.*, 168:464–499, 2001.

- [7] A. J. Chorin. Numerical solution of the Navier Stokes equations. *Math. Comp.*, 22:745–762, 1968.
- [8] R.K. Crockett, P. Colella, and D.T. Graves. A cartesian grid embedded boundary method for solving the poisson and heat equations with discontinuous coefficients in three dimensions. *Journal of Computational Physics*, 230(7):2451–2469, 2010.
- [9] Jian Du, Brian Fix, James Glimm, Xicheng Jia, Xiaolin Li, Yunhua Li, and Lingling Wu. A simple package for front tracking. *J. Comput. Phys.*, 213:613–628, 2006.
- [10] D.E. Fyfe, E.S. Oran, and M.J. Fritts. Surface tension and viscosity with lagrangian hydrodynamics on a triangular mesh. *J. Comput. Phys.*, 76:349–384, 1988.
- [11] J. Glimm, J. W. Grove, X.-L. Li, K.-M. Shyue, Q. Zhang, and Y. Zeng. Three dimensional front tracking. *SIAM J. Sci. Comput.*, 19:703–727, 1998.
- [12] J. Glimm, D. Marchesin, and O. McBryan. *J. Comput. Phys.*, 39:179,200.
- [13] Kazufumi Ito and Zhilin Li. Interface conditions for Stokes equations with a discontinuous viscosity and surface sources. *Applied Mathematics Letters*, 19:229–234, 2006.
- [14] H. Johansen and P. Colella. A cartesian grid embedding boundary method for poisson’s equation on irregular domains. *J. Comput. Phys.*, 147:60–85, 1998.
- [15] James Edward Pilliod Jr. and Elbridge Gerry Puckett. Second-order accurate volume-of-fluid algorithms for tracking material interfaces. *Journal of Computational Physics*, 199:465–502, 2004.
- [16] M. Kang, R. Fedkiw, and X.-D. Liu. A boundary condition capturing method for multiphase incompressible flow. *J. Sci. Comput.*, 15(3):323–360, 2000.
- [17] Ming-Chin Lai and Zhilin Li. A remark on jump conditions for the three-dimensional Navier-Stokes equations involving an immersed moving membrane. *Applied Mathematics Letters*, 14:149–154, 2001.
- [18] L. Lee and R. LeVeque. An immersed interface method for incompressible navier-stokes equations. *SIAM J. Sci. Comput.*, 25(3):832–856, 2003.
- [19] R.J. LeVeque and Z.L. Li. The immersed interface method for elliptic equations with discontinuous coefficients and singular sources. *SIAM J. Numer. Anal.*, 31:1019–1044, 1994.
- [20] Z. Li and K. Ito. *The Immersed Interface Method: Numerical Solutions of PDEs Involving Interfaces and Irregular Domains*. Frontiers Appl. Math. 33, SIAM, Piladelphia, 2006.

- [21] Hongyu Liu and Jun Zou. Some new additive runge-kutta methods and their applications. *Journal of Computational and Applied Mathematics*, 190:74–98, 2006.
- [22] X.-D. Liu, R. Fedkiw, and M. Kang. A boundary condition capturing method for poisson’s equation on irregular domains. *J. Comput. Phys.*, 160:151–178, 2000.
- [23] W. E. Lorensen and H. E. Cline. Marching cubes: A high resolution 3D surface construction algorithm. *Computer Graphics*, 21(4):163–169, 1987.
- [24] P. McCorquodale, P. Colella, and H. Johansen. A cartesian grid embedded boundary method for the heat equation on irregular domains. *J. Comput. Phys.*, 173:620–635, 2001.
- [25] G. H. Miller and D. Trebotich. An embedded boundary method for the navier-stokes equations on a time-dependent domain. *Communications in Applied Mathematics and Computational Science*, 7(1):1–31, 2012.
- [26] Stanley J. Osher and Ronald P. Fedkiw. *Level Set Methods and Dynamic Implicit Surfaces*. Springer, 2002.
- [27] Charles S. Perskin. The immersed boundary method. *Acta Numerica*, 11:479–517, 2002.
- [28] Elbridge G. Puckett, , Ann S. Almgren, John B. Bell, Daniel L. Marcus, and William J. Rider. A high-order projection method for tracking fluid interfaces in variable density incompressible flows. *Journal of Computational Physics*, 130:269–282, 1997.
- [29] Peter Schwartz, Michael Barad, Phillip Colella, and Terry Ligoeki. A cartesian grid embedded boundary method for the heat equation and poisson’s equation in three dimensions. *J. Comput. Phys.*, 211:531–550, 2006.
- [30] J. A. Sethian. *Level Set Methods and Fast Marching Methods: Evolving Interfaces in Computational Geometry, Fluid Mechanics, Computer Vision, and Materials Science*. Cambridge University Press, 1999.
- [31] S. Shin and D. Juric. Modeling Three-Dimensional Multiphase Flow Using a Level Contour Reconstruction Method for Front Tracking without Connectivity. *J. Comput. Phys.*, 180:427–470, August 2002.
- [32] M. Sussman and P. Smereka. Axisymmetric free boundary problems. *J. Fluid Mech.*, 341:269–294, 1997.
- [33] Mark Sussman, Peter Smereka, and Stanley Osher. A level set approach for computing solutions to incompressible two-phase flow. *Journal of Computational Physics*, 114:146–159, 1994.

- [34] Zhijun Tan, D.V. Le, K.M. Lim, and B.C. Khoo. An immersed interface method for the incompressible navier-stokes equations with discontinuous viscosity across the interface. *SIAM J. Sci. Comput.*, 31:1798–1819, 2009.
- [35] G. Tryggvason, B. Bunner, and et. al. A front-tracking method for the computations of multiphase flow. *J. Comput. Phys.*, 169:708–759, 2001.
- [36] E.H. Twizell, A.B. Gumel, and M.A. Arigu. Second-order, l0-stable methods for the heat equation with time-dependent boundary conditions. *Adv. Comput. Math.*, 6:333–352, 1996.
- [37] S. O. Unverdi and G. Tryggvason. A front-tracking method for viscous, incompressible, multi-fluid flows. *J. Comput. Phys.*, 100(1):25–37, 1992.
- [38] S. Wang and J. Glimm. 3d volume calculation for the marching cubes method in cartesian/cylindrical coordinates. in preparation, 2012.
- [39] Shuqiang Wang, Roman V Samulyak, and Tongfei Guo. An embedded boundary method for elliptic and parabolic problems with interfaces and application to multi-material systems with phase transitions. *Acta Mathematica Scientia*, 30B(2).
- [40] Y. Zhou, N. Ray, H. Lim, S. Wang, V. F. de Almeida, J. Glimm, X.-L. Li, and X. Jiao. Development of a front tracking method for two-phase micromixing of incompressible viscous fluids with interfacial tension in solvent extraction. Technical Report ORNL/TM-2012/28, Oak Ridge National Laboratory, 2012.

A Approximate Jump Conditions for Decoupling Velocity

This part is modified from [16]. Instead of using the jump condition (16), we can use any equivalent jump conditions. Due to the incompressibility condition $\nabla \cdot u = 0$, we have $[\mu \nabla \cdot u] = 0$, which can also be written as (Zhi, et al [34])

$$[\mu \frac{\partial u}{\partial n}] \cdot n + [\mu \frac{\partial u}{\partial \tau_1}] \cdot \tau_1 + [\mu \frac{\partial u}{\partial \tau_2}] \cdot \tau_2 = 0 \quad (32)$$

Equations (15,32) can be written in matrix notation in 3D as the following:

$$\begin{pmatrix} n \\ \tau_1 \\ \tau_2 \end{pmatrix} [\mu \frac{\partial u}{\partial n}] + \begin{pmatrix} \tau_1 \\ n \\ 0 \end{pmatrix} [\mu \frac{\partial u}{\partial \tau_1}] + \begin{pmatrix} \tau_2 \\ 0 \\ n \end{pmatrix} [\mu \frac{\partial u}{\partial \tau_2}] + \begin{pmatrix} 0 \\ \tau_1 \\ \tau_2 \end{pmatrix} f = 0 \quad (33)$$

Multiplying both sides of this equation from the left by

$$\begin{pmatrix} n \\ \tau_1 \\ \tau_2 \end{pmatrix}^T,$$

we have

$$\begin{aligned} [\mu \frac{\partial u}{\partial n}] + \begin{pmatrix} n \\ \tau_1 \\ 0 \end{pmatrix}^T \begin{pmatrix} \tau_1 \\ n \\ 0 \end{pmatrix} [\mu \frac{\partial u}{\partial \tau_1}] + \begin{pmatrix} n \\ 0 \\ \tau_2 \end{pmatrix}^T \begin{pmatrix} \tau_2 \\ 0 \\ n \end{pmatrix} [\mu \frac{\partial u}{\partial \tau_2}] \\ + \begin{pmatrix} 0 \\ \tau_1 \\ \tau_2 \end{pmatrix}^T \begin{pmatrix} 0 \\ \tau_1 \\ \tau_2 \end{pmatrix} f = 0 \end{aligned}$$

Since the tangential derivative of the velocity is continuous ([17], [16]), we have

$$[\mu \frac{\partial u}{\partial n}] + [\mu] \begin{pmatrix} n \\ \tau_1 \\ 0 \end{pmatrix}^T \begin{pmatrix} \tau_1 \\ n \\ 0 \end{pmatrix} \frac{\partial u}{\partial \tau_1} + [\mu] \begin{pmatrix} n \\ 0 \\ \tau_2 \end{pmatrix}^T \begin{pmatrix} \tau_2 \\ 0 \\ n \end{pmatrix} \frac{\partial u}{\partial \tau_2} \quad (34)$$

$$+ \begin{pmatrix} 0 \\ \tau_1 \\ \tau_2 \end{pmatrix}^T \begin{pmatrix} 0 \\ \tau_1 \\ \tau_2 \end{pmatrix} f = 0 \quad (35)$$

Thus if the surface force f has no or very small tangential components (as in surface tension force) and $[\mu]$ is very small, it is safe to approximate the jump conditions of the velocity using

$$[\mu \frac{\partial u}{\partial n}] = 0 \quad (36)$$

At an interior point away from the interface, we have $[\mu] = 0$ and $f = 0$, therefore $[\mu \frac{\partial u}{\partial n}] = 0$.

B Code Structure and Parallelization

In this section, we briefly introduce the data structure, coding for dealing with partial cells, and the parallelization method used for the EBM. For simplicity, we use 2D as example.

The EBM uses a structured Cartesian mesh. For a 2D rectangle domain, we use a two dimensional array to represent the Cartesian mesh. We need to store extra geometric information for partial cells (partial area, cell interface length, center, normal) and partial cell edge (length, center). We also need to store extra states for the partial cells and partial cell edges. Since the data size needed for partial cells with internal interface is much larger than the data size needed for a regular internal cell, we use an extra pointer to a data structure for the partial cells (called partial cell data structure later on). The extra data structure is allocated and deallocated dynamically. A cell type variable is maintained for each cell to distinguish between internal, partial, external and boundary cell (cell with external boundary crossing through). For a moving interface, the cell type could change dynamically. For the cell edge, the same data structure is

used for both whole and partial cell edges since a partial cell edge needs only a few extra data storage.

Whenever the interface is changed, the partial cells are identified and the partial cell data structures are set. The partial cell geometric information is calculated using cell corner component and cell edge crossing information using the Marching Cubes algorithm [23, 38] (with the assumption that there is at most one crossing at each cell edge). The geometric information for the partial cell edge is also set accordingly.

The EBM is a finite volume method. A systematic way of enumerating the cell internal interface and the partial cell edges is used to calculate the flux of the differential equations.

Due to the structured Cartesian mesh used, it is very easy to parallelize the code. There are three types of variables: cell center variables (cell center velocities, pressure), cell face variables (cell face velocities), and cell corner variables. The parallelization consists of three steps: 1) pack; 2) send/receive; 3) unpack. The unpack step is just the reverse step of the pack step. We first allocate a big array. Then for each cell to be sent, we first pack the cell type, and then pack all other variables associated with that cell into the array. Then we send/receive the single array. The unpack process is similar with the pack process. For each cell in the buffer zone, we first get the cell type from the received array, and then unpack the other variables.